A doubly fed induction generator using back-to-back PWM converters supplying an isolated load from a variable speed wind turbine

Article *in* IEE Proceedings - Electric Power Applications · October 1996

DOI: 10.1049/ip-epa:19960454 · Source: IEEE Xplore

3 authors, including:

R. Pena
University of Concepción
124 PUBLICATIONS **5,888** CITATIONS
SEE PROFILE

Jon C Clare
University of Nottingham
431 PUBLICATIONS **13,173** CITATIONS
SEE PROFILE

A doubly fed induction generator using back-to-back PWM converters supplying an isolated load from a variable speed wind turbine

R.Pena
J.C.Clare
G.M.Asher

Indexing terms: Doubly fed induction motor, PWM converters, Vector control, Wind energy

Abstract: A doubly fed induction generator (DFIG) designed to be driven at variable speed from a wind turbine and supplying an isolated load is presented. Two back-to-back PWM voltage-fed inverters connected between the stator and the rotor allow sub- and super-synchronous operation with low distortion currents. The load voltage is maintained at constant frequency and its magnitude is regulated through control of the stator flux of the generator. An auxiliary load is connected in parallel with the main load, and the auxiliary power is controlled to allow the DFIG to track the optimal wind turbine speed for maximum energy capture from the wind. An indirect stator-orientated vector control scheme is used to control the DFIG and this results in constant load voltage and frequency for variations in both load and wind speed. The techniques have been implemented and validated on a 7.5kW experimental rig.

List of symbols

v_{ds}, v_{qs}, v_{dr}, v_{qr} = 2-axis machine voltages
i_{ds}, i_{qs}, i_{dr}, i_{qr} = 2-axis machine currents
λ = flux linkage
L_s, L_r, L_o, L_m = machine inductances per phase
R_s, R_r = machine resistances per phase
σ_s = leakage factor
i_{ms} = magnetising current referred to stator
T_{ms} = stator time constant
p = pole pairs
ω_e, ω_r = supply, rotor angular frequency
θ_r = rotor position
θ_e = stator flux angle
θ_v = stator voltage angle
θ_{slip} = slip angle
s = slip
T_e = electromagnetic torque
T_{opt} = optimum torque
P_{opt} = optimum power
δ = chopper duty cycle
v = wind velocity
B = friction coefficient

Suffices

d, q = d–q (synchronous) axes
α, β = α, β (stationary) axes
s, r = stator, rotor

Superscripts

* = demanded (reference) value

IEE Proceedings online no. 19960454

Paper first received 2nd November 1995 and in revised form 11th March 1996

The authors are with the Department of Electrical and Electronic Engineering, The University of Nottingham, University Park, Nottingham NG7 2RD, UK

1 Introduction

The doubly fed induction generator (DFIG) can supply power at constant voltage and constant frequency while the rotor speed varies. This makes it suitable for variable speed wind energy applications. Additionally, when a bidirectional AC–AC converter is used in the rotor circuit, the speed range can be extended above synchronous speed and power can be generated both from the stator and the rotor. An advantage of this type of DFIG drive is that the rotor converter need only be rated for a fraction of the total output power, the fraction depending on the allowable sub- and super-synchronous speed range.

A good introduction to the operational characteristics of the DFIG connected to the grid can be found in [1, 2] in which Scherbius schemes using either cycloconverters or six pulse naturally commutated DC-link converters are used. Problems affect one or both types of converter: restricted speed range, extra forced commutation at synchronous speed and poor quality converter currents. These may be overcome by using back-to-back PWM converters in the rotor circuit. Such converters are characterised by low distortion currents both in the machine rotor and the supply grid. They also provide control of the overall system power factor. A grid-connected DFIG system using such a scheme has been simulated in [3] and shown to be experimentally feasible [4]. A full experimental investigation of the grid-connected scheme has been done by the present authors [5] who have demonstrated the excel-

lent dynamic performance of the vector control schemes regulating the system power factor and the converter link voltage while providing for maximum energy generation under variable wind speed conditions.

The possibility of a DFIG supplying an isolated load has been indicated in [6, 7] in which some mention is made of the steady state control problem. In [8] results from a simulation are presented in which the stator voltage is controlled directly rather than via a field orientated stator flux controller such as that used in the present study. Direct control of the stator voltage leads to considerable practical difficulties (which are overcome with flux control) since the control characteristics are load dependent. In [9] a system is presented in which the rotor is supplied from a battery via a PWM converter with experimental results from a 250W prototype. A control system based on regulating the rms voltage is used which results in large voltage deviations and very slow recovery following load changes. Again, the control design is load dependent. In [10] Joeng and Park present a working scheme for a DFIG supplying an isolated load. This system is unable to operate super-synchronously and the harmonic currents drawn by the diode rectifier are undesirable. Only steady state results are shown.

This paper presents the analysis, control and experimental validation of a vector controlled variable speed DFIG supplying an isolated load. Two back-to-back PWM voltage-fed inverters connected between the stator and the rotor are used to allow bidirectional power flow. A novel indirect stator flux orientation is proposed for vector control of the generator in which the stator flux angle is not derived from voltage measurement and is thus shielded from noise and possible harmonic contamination on the stator voltage. This angle is also used to derive the voltage vector orientation for vector control of the supply-side PWM converter. The experimental validation of the scheme is presented first with the generator driven by a speed controlled DC motor at both sub- and super-synchronous speeds. Under steady speed conditions, the output regulation performance is investigated for impact changes in both active and reactive load. For investigating the performance under variable speed, an auxiliary load control system is presented and the DC motor operated under torque control so as to emulate a wind turbine. Dynamic results are presented illustrating the regulation of output voltage and frequency under load impacts and variable wind speed while maintaining maximum energy capture from the wind.

2 Experimental system

A schematic of the overall system feeding an isolated load is shown in Fig. 1. The system shown is in fact a modified version of the grid-connected system described by the authors in [5] and the reader is referred to that work for a complete description and a discussion of the selection of the rated operating points.

The DFIG used was a 7.5kW, 415V, 50Hz 6-pole machine whose parameters are given in the Appendix. The PWM converters used were standard 7.5kW commercial bipolar transistor PWM inverters with a maximum switching frequency of 1kHz. For all of the experimental investigations the DC-link voltage was set at 550V and the DFIG was operated with a reduced voltage of 220V because of the voltage limitation of the converters [5]. The inclusion of line inductance in the rotor circuit is explained in [5]. The turbine and gearbox is emulated in the experimental system by a thyristor converter fed DC machine which simulates a 7.5kW turbine with cut-in and rated wind speeds of $4ms^{-1}$ and $10ms^{-1}$, respectively, corresponding with generator speeds of 500 and 1500rpm.

The DC motor was a 15kW, 1500rpm machine operated under either speed or torque control. Under torque control, wind speed data is fed from a PC to a microprocessor which calculates the instantaneous turbine torque from a given turbine blade characteristic (see the Appendix). This torque forms the torque demand to the DC drive after compensation for drive losses. The speed of the turbine-generator set is determined by an optimal speed tracking algorithm that effects maximum energy capture from the wind. When the generated power exceeds the load power under these conditions, the surplus power is dumped in an auxiliary load. The exact nature of an auxiliary load depends on the stand-alone application; resistive heating and water pumping for irrigation are two common examples. In this study, the auxiliary load is a diode

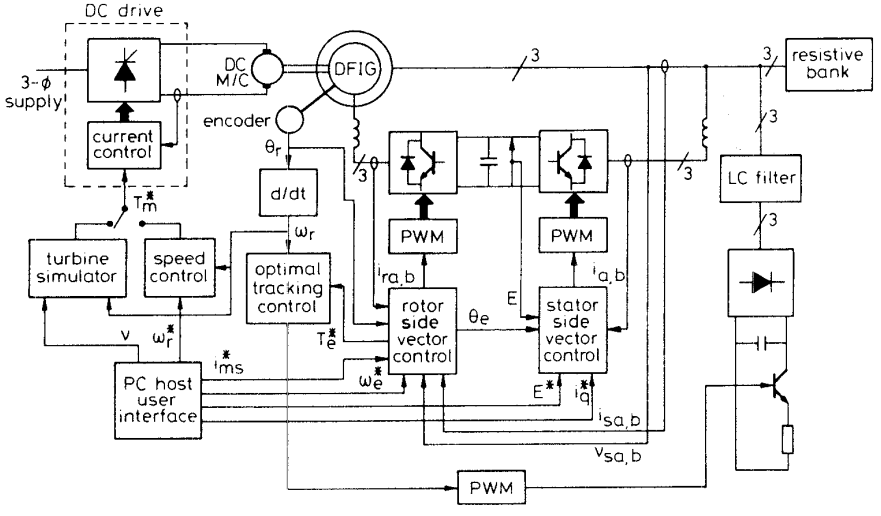

Fig. 1 *Schematic of stand-alone variable speed wind generation system*

rectifier with an input filter feeding a chopper controlled resistive load. The main load is a 3-phase switched resistance bank.

Other system set points input from the PC include the DC-link voltage, the reactive current drawn by the supply-side PWM converter (which is used in this study to emulate the existence of an inductive load), the stator frequency and the stator magnetising current (which determines the stator output voltage). The microprocessors used in the experimental rig were T800 floating point transputers; further details may be found in [5]. Two high-performance microcontrollers (e.g. the SAB 166) could have been used. The PWM switching frequency was set at 1kHz on account of the converters used. The sampling period for all currents and voltages, and all control loops was 500μs unless specified otherwise.

3 Vector control of the induction generator

The DFIG must supply constant voltage and frequency at the stator terminals irrespective of the shaft speed. Unlike the grid-connected case [5], the stator flux is no longer determined by the grid voltage and is thus set by regulating the rotor excitation current. A decoupled orthogonal control using field-oriented techniques can be used leading to direct control of the stator flux by one of the rotor current components.

The machine equations written in a synchronously rotating d–q reference frame are:

$$\begin{aligned}
\lambda_{ds} &= L_s i_{ds} + L_o i_{dr} = L_o i_{ms} \\
\lambda_{qs} &= L_s i_{qs} + L_o i_{qr} \\
\lambda_{dr} &= L_o i_{ds} + L_r i_{dr} \\
\lambda_{qr} &= L_o i_{qs} + L_r i_{qr} \\
v_{ds} &= R_s i_{ds} + \frac{d\lambda_{ds}}{dt} - \omega_e \lambda_{qs} \\
v_{qs} &= R_s i_{qs} + \frac{d\lambda_{qs}}{dt} + \omega_e \lambda_{ds} \\
v_{dr} &= R_r i_{dr} + \frac{d\lambda_{dr}}{dt} - (\omega_e - \omega_r)\lambda_{qr} \\
v_{qr} &= R_r i_{qr} + \frac{d\lambda_{qr}}{dt} + (\omega_e - \omega_r)\lambda_{dr}
\end{aligned} \tag{1}$$

where i_{ms} is the equivalent stator magnetising current. Aligning the d-axis of the reference frame on the stator flux vector gives:

$$i_{qr} = -\frac{L_s}{L_o} i_{qs} \tag{2}$$

Eliminating i_{ds} using the definition for i_{ms} given in eqn. 1 and eliminating i_{qs} using eqn. 2 yields, with $\lambda_{qs} = 0$:

$$T_{ms}\frac{di_{ms}}{dt} + i_{ms} = i_{dr} + \frac{1+\sigma_s}{R_s} v_{ds} \tag{3}$$

$$T_{ms} i_{ms} \omega_e = i_{qr} + \frac{1+\sigma_s}{R_s} v_{qs} \tag{4}$$

where $T_{ms} = L_s/R_s$. Eqn. 3 shows that, since the influence of v_{ds} is small, i_{ms} can be controlled using i_{dr}. The rotor current i_{qr} constitutes a degree of freedom and can be controlled via

$$i_{qr}^* = -\frac{L_s}{L_o} i_{qs} \tag{5}$$

to force the orientation of the reference frame along the stator flux vector position. Only when $\lambda_{qs} = 0$ is eqn. 5 valid, and it is assumed that i_{qr} follows i_{qr}^* under the action of a fast control loop. Eqn. 4 could also be used to force the orientation but this is not a good approach in practice since i_{qr} is given by the difference between two larger quantities which are subject to noise. The orientation condition (eqn. 5) also means that the stator flux angle does not have to be derived from integration of the stator voltages, but can be derived directly from a free running integral of the stator voltage frequency demand ω_e^* (50Hz). This has the advantage that the orientation is shielded from measurement noise and stator voltage harmonics which may be a problem in a stand-alone application if a converter controlled auxiliary load is used (see Section 6). With this indirect orientation scheme, i_{qr} can no longer be used to control the generator torque; this is entirely appropriate for the stand-alone application in which the power control of an auxiliary load effectively determines the torque for a given shaft speed.

The vector control schematic is shown in Fig. 2. The current components i_{dr} and i_{qr} are controlled in the d–q axis through PI controllers. The PI controller design and the derivation of the terms compensating the rotor back emf are described in [5]. The demodulation of the

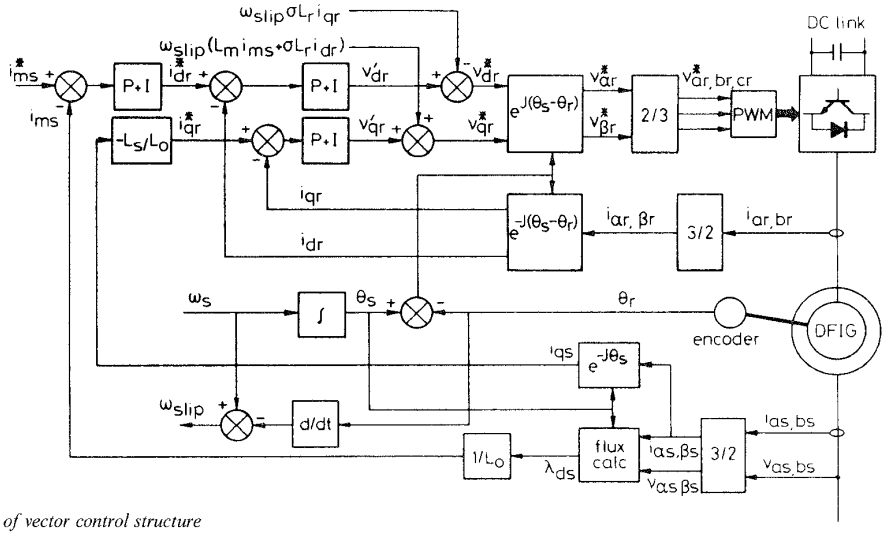

Fig. 2 *Schematic of vector control structure*

rotor demand voltages uses the slip angle derived from:

$$\theta_{slip} = \theta_e - \theta_r = \int \omega_e^* dt - \theta_r \tag{6}$$

where θ_r is measured using a 720-line encoder. Eqn. 6 forces the stator flux to rotate at the demand frequency during both steady state and dynamic conditions for any shaft speed.

3.1 Stator flux and voltage regulation

Stator flux is regulated through control of i_{ms}. This is obtained from:

$$i_{ms} = \frac{\lambda_{ds}}{L_o} \tag{7}$$

$$\lambda_{ds} = \lambda_{\alpha s} \cos\theta_e + \lambda_{\beta s} \sin\theta_e$$

$$\lambda_{\alpha s} = \int (v_{\alpha s} - R_s i_{\alpha s}) dt \tag{8}$$

$$\lambda_{\beta s} = \int (v_{\beta s} - R_s i_{\beta s}) dt$$

where α, β denotes the stationary reference frame. The angle θ_e is used to demodulate both the stator flux and the stator currents although i_{ds} is not used. The derived i_{ms} is compared with the demand value and the error forms the command i_{dr}^* via a PI controller as shown in Fig. 2. The i_{ms} loop, shown in Fig. 3, was designed with a closed-loop natural frequency of 6.7rads^{-1}. This is limited by the available converter voltage.

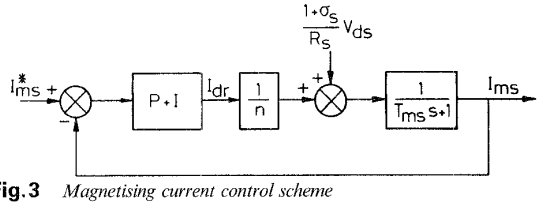

Fig.3 *Magnetising current control scheme*

In the present implementation, the magnetising current demand i_{ms}^* is set directly from the user PC and the stator voltage is not compensated against load variations (the uncompensated steady state voltage regulation is about 3% for maximum load which is considered acceptable for the purposes of the present investigation). For all of the experimental investigations, i_{ms}^* was set to 6A corresponding to a stator voltage of 220V. More effective regulation could be obtained deriving i_{ms}^* from the v_{qs} equation in eqn. 1 taking into account the stator resistance. Under dynamic loads, the voltage regulation will have the same bandwidth as the i_{ms} loop; this is of course unavoidable.

4 Vector control of the stator side converter

The vector control of the stator side (front-end) converter uses a reference frame oriented along the stator voltage vector position. The analysis and implementation is fully described in [5]. Under stator voltage orientation, the direct component of the AC side converter current, i_d, is proportional to the rotor power and is used as the actuating variable in a DC-link voltage control loop, the DC-link voltage reference being set by the user from the PC. The quadrature current component, i_q, represents the reactive power and directly determines the displacement factor of the converter current. In a stand-alone application, any reactive current drawn by the load must be supplied either by the stator or the stator converter. If supplied by the stator, the rotor excitation current, i_{dr}, will naturally compensate under the action of the i_{ms} loop described in the previous section. This is investigated experimentally in Section 5. Sourcing the reactive power from the stator converter can be achieved by forming the i_q^* demand from the i_{ms} PI controller; this can be done after the i_{qr}^* demand reaches a given limit (and then held at that limit); or alternatively the i_{ms} PI controller output may supply both demands through a sharing algorithm. The optimum source of reactive power will depend on relative loss considerations in the machine and the two converters and is beyond the scope of this paper. In this study i_q^* is normally set to zero.

A complication arising from the stand-alone application concerns the derivation of the voltage vector position angle, θ_v, for the stator converter. In a grid-connected application, the grid voltages may be assumed to be free of harmonics and θ_v is derived through voltage measurements as described in [5]. In the stand-alone case, there is no low impedance voltage source and stator voltage harmonics will predominantly arise from the PWM voltage harmonics of the stator converter and from the current harmonics drawn by a converter controlled auxiliary load. It has been determined through experimental investigation that, even with the LC line filters of Section 2 included, these voltage harmonics are amplified to an unacceptable degree if the voltage angle θ_v is calculated from voltage measurement. Fortunately, the angle θ_v may be derived from:

$$\theta_v = \theta_e + \pi/2 \tag{9}$$

where θ_e is derived from the frequency reference which is a clean software variable. The error in θ_v due to the DFIG stator impedance voltage drop under load is negligible in practice. The resulting viability of the stator side converter operation is a significant advantage of the indirect orientation scheme described in Section 3.

5 Experimental results without auxiliary load

For this study the DFIG was driven by the DC machine under speed control. The DFIG was subject to step changes in active load power and reactive load power with the generator driven at both sub- and super-synchronous speeds.

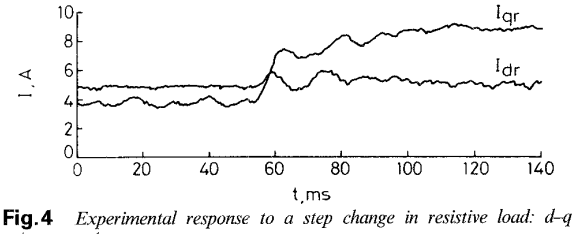

Fig.4 *Experimental response to a step change in resistive load: d–q rotor current*

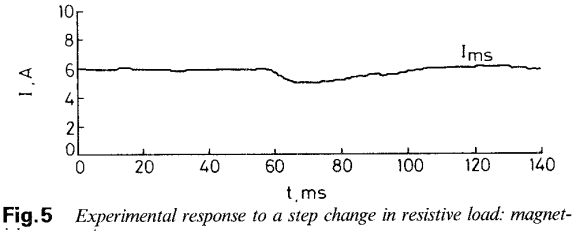

Fig.5 *Experimental response to a step change in resistive load: magnetising current*

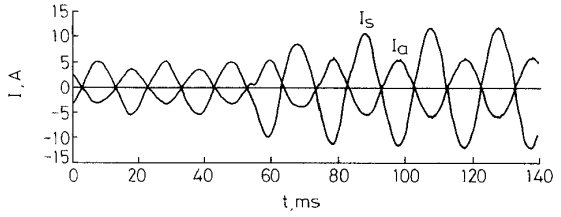

Fig. 6 *Experimental response to a step change in resistive load: stator current; front-end converter current*

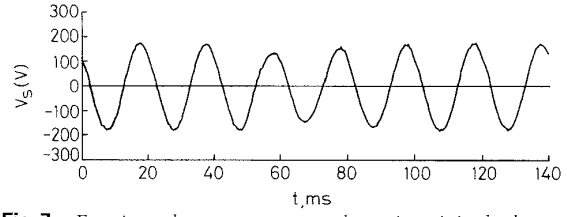

Fig. 7 *Experimental response to a step change in resistive load: stator voltage*

Figs. 4–7 show the response to a step change in the active load power from 550W to 1650W (approx 15% to 40% of rated load with the reduced line voltage) with the speed at 700rpm (s = 0.3). Fig. 4 shows the d–q axis motor currents. After the impact there is a momentary loss of field orientation due to the finite response time of the i_{qr} loop; the loss of orientation reduces the i_{qs} component at the expense of a negative i_{ds} component that serves to reduce the magnetising current, as shown in Fig. 5, and hence the voltage. The orientation recovers in about 40ms (this does not relate to the response speed of the i_{qr} loop because of the reduction in i_{qs} and hence i_{qr}^*). Fig. 6 shows that the increase in i_{qr} draws an increase in active power through the rotor circuit resulting in an increase in the front-end converter current which is of course expected at sub-synchronous speed. Fig. 7 shows the corresponding voltage dip lasting barely one cycle. Both the magnitude and duration of the dip can be reduced through increasing the speed of the current loops.

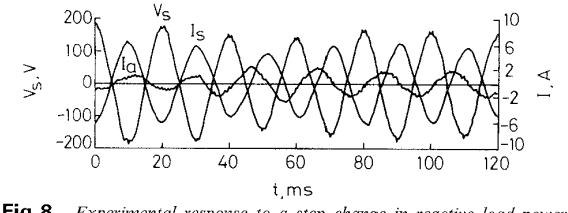

Fig. 8 *Experimental response to a step change in reactive load power: stator voltage, stator current and magnetising current*

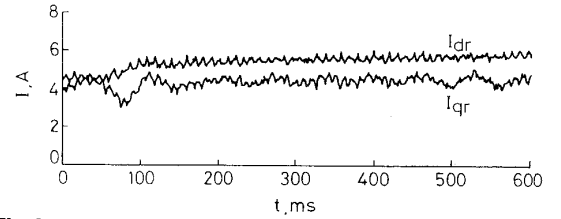

Fig. 9 *Experimental response to a step change in reactive load power: d–q axis rotor currents*

Figs. 8–10 show the response to a step change in reactive (inductive) load. This was emulated through a step i_q^* demand of 0A to 3A in the front-end converter so that it no longer operates at unity displacement factor. The speed is 1300rpm (s = –0.3). Fig. 8 shows the phase relationship of the front-end converter current, I_a, and machine stator current, I_s, with respect to the voltage. Following the impact the stator supplies reactive power which de-fluxes the machine since i_{ms} can not respond immediately. The excitation level is restored under the action of the slow i_{ms} loop which increases i_{dr} as shown in Figs. 9 and 10. As before, there is a small disturbance in i_{ms} and i_{qr} immediately after the impact which is evidence of a momentary loss of orientation.

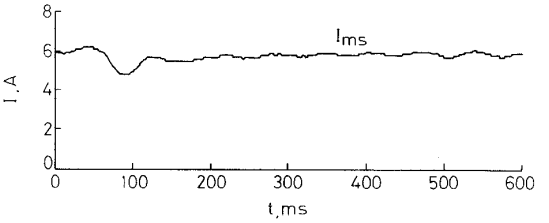

Fig. 10 *Experimental response to a step change in reactive load power: magnetising current*

6 Optimal wind turbine operation using auxiliary load

When the generator is driven by a wind turbine it will be necessary to match the power extracted from the wind with the isolated load power and the electrical and mechanical power loss. Fig. 11 shows the turbine power–shaft speed characteristics (for various wind speeds) of the 7.5kW wind turbine emulated with the DC drive. The maximum energy capture curve (P_{opt} in Fig. 11) for below rated wind speed operation (BRWS) is defined by

$$P_{opt} = K_{opt}\omega_r^3 \qquad T_{opt} = K_{opt}\omega_r^2 \tag{10}$$

where K_{opt} is a function of blade parameters. To ensure the system operates on the maximum energy capture curve, an auxiliary load is used to make up the difference between the optimum power and the main load power. For wind speeds higher than rated, the turbine energy capture must be limited by using pitch control or stall control [11].

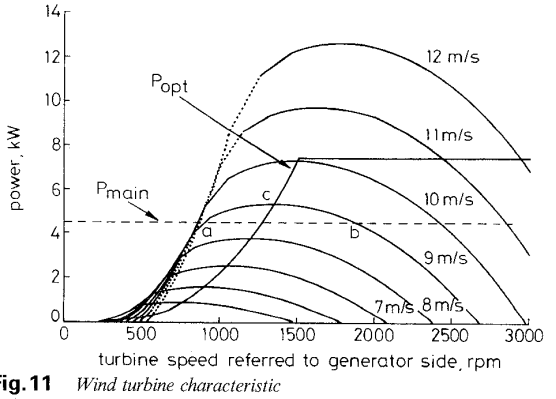

Fig. 11 *Wind turbine characteristic*

In this study, the auxiliary load is a diode rectifier (with an input filter) feeding a chopper-controlled resistive load (Fig. 1). This was chosen for experimental convenience but represents a situation where converter fed auxiliary loads may well be a practical option (battery charging, variable speed irrigation pumps, etc.).

6.1 Control of the auxiliary load power

The proposed control is shown in Fig. 12. The shaft speed is measured and the generator torque demand, T_e^* set according to

$$T_e^* = K_{opt}\omega_r^2 - B\omega_r \tag{11}$$

where B represents a linear approximation to the friction coefficient. The generator torque is calculated from

$$T_e = 3\frac{p}{2}L_m i_{ms} i_{qr} \qquad L_m = L_o^2/L_s \tag{12}$$

and the error between T_e and T_e^* processed by a PI controller to form the duty cycle command for the auxiliary load chopper. A change in the main load is reflected in a change in i_{qs}, hence i_{qr} and T_e. This is represented by a change in i_{qr}^{main} in Fig. 12. The optimal torque is maintained by an appropriate compensating auxiliary load demand. Eqn. 11 is always satisfied in steady state, ensuring maximum energy capture. The success in tracking the optimal power–speed curve under changing wind conditions is dependent on the rate of wind speed changes and the turbine and drive train inertia [12, 13].

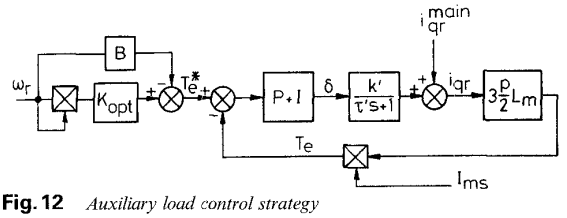

Fig. 12 *Auxiliary load control strategy*

The auxiliary load dynamics are difficult to determine analytically. A crude approximation has been made by assuming a first-order response between the chopper duty cycle (δ) and i_{qr}. This implies a first-order response between δ and T_e given at zero main load by

$$\frac{T_e(s)}{\delta(s)} = \frac{3\frac{p}{2}L_m I_{ms} k'}{\tau' s + 1} \tag{13}$$

which can be found by experiment from a step response test. From several tests the best first-order fit to the transfer function was found to be

$$\frac{T_e(s)}{\delta(s)} = \frac{1.26}{0.25s + 1} \tag{14}$$

A PI controller was designed to give a well-damped response with natural frequency 3rads^{-1}. The sampling time for this loop was 5ms.

7 Experimental results for variable speed wind turbine using auxiliary load

Validation of the proposed scheme was carried out for step changes in wind velocities and changes in the main load supplied by the generator.

Figs. 13–15 show the performance of the generator for an increase in wind speed from 6ms^{-1} to 9ms^{-1}; this corresponds to 'maximum energy capture' shaft speeds of 900rpm (sub-synchronous) and 1350rpm (super-synchronous). The main load draws a constant 200W. Fig. 13 illustrates the increase in i_{qr} resulting from the increase in auxiliary load power while i_{ms} is held constant. The increase in i_{dr} is due to the auxiliary load LC filter drawing increasing reactive (inductive) power as the auxiliary load power increases. The speed transient rate in Fig. 14 is determined by the system inertia which for the experimental rig was 7.5kgm^2; this is actually rather large for a 7.5kW rating. Fig. 14 also shows the chopper duty cycle which increases under the action of the optimal tracking control to increase the auxiliary load power. Fig. 15 shows the corresponding power flows in the system during the step wind change. Below synchronism, the rotor power is directed into the rotor and is therefore supplied from the stator, circulating via the front-end and rotor converters. Fig. 16 shows the transition through synchronous speed illustrating that proper control over the rotor current is maintained at all times. Figs. 17 and 18 show the response to step changes in main load of 600W–1680W–600W for a speed of 1300rpm (s = –0.3). From Fig. 12 it is seen that the duty cycle and i_{qr} are the step and impulse responses of the torque loop respectively. This is verified in Figs. 17 and 18. The change in i_{dr} again reflects the change in reactive power drawn by the LC filter associated with the auxiliary load; there is also a small (≈6%) disturbance in i_{ms} during the impacts which illustrates the good quality of the field orientation. Figs. 19 and 20 show the response to a step change in main load power (600W to 1680W) which occurs while the system is tracking to a new optimum speed following a change in wind velocity (7ms^{-1} to 9ms^{-1}). The system is able to cope with this more difficult situation without any undesirable interaction between the control loops.

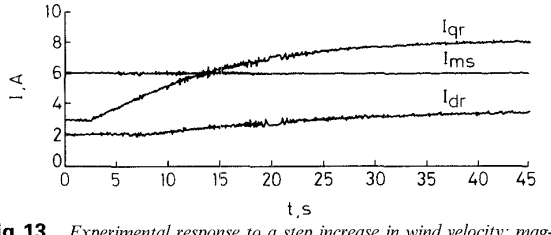

Fig. 13 *Experimental response to a step increase in wind velocity: magnetising current, d-q axis rotor currents*

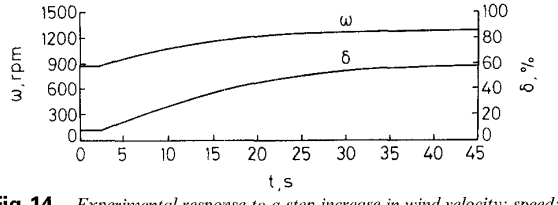

Fig. 14 *Experimental response to a step increase in wind velocity: speed; auxiliary load duty cycle*

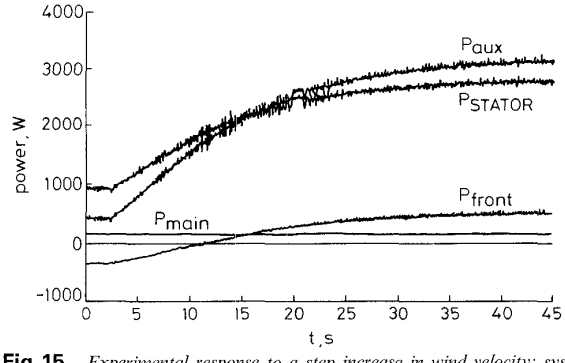

Fig. 15 *Experimental response to a step increase in wind velocity: system power flow*

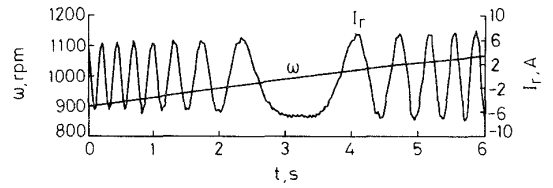

Fig. 16 *Experimental results for operation through synchronous speed*

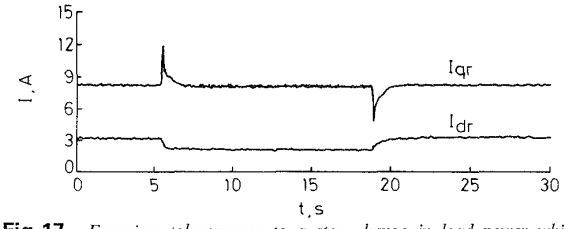

Fig. 17 *Experimental response to a step change in load power while operating at constant (optimum) speed: d–q axis rotor currents*

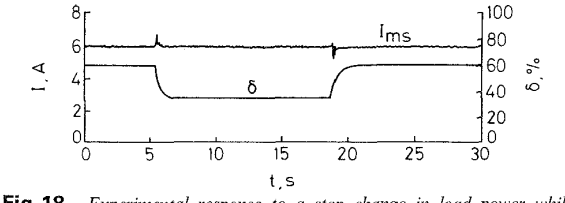

Fig. 18 *Experimental response to a step change in load power while operating at constant (optimum) speed: magnetising current; auxiliary load duty cycle*

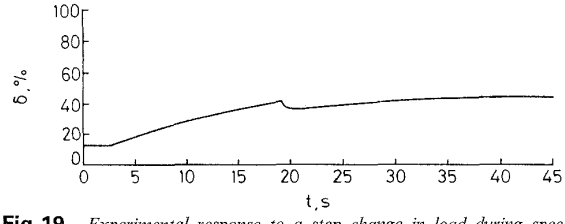

Fig. 19 *Experimental response to a step change in load during speed tracking: auxiliary load duty cycle*

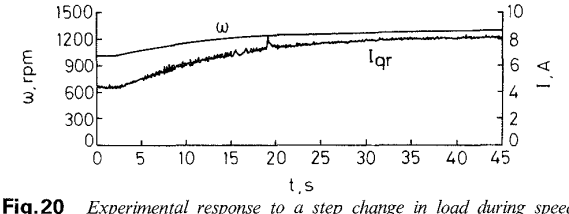

Fig. 20 *Experimental response to a step change in load during speed tracking: speed and q-axis rotor current*

The ability of the system to maintain constant output voltage during real wind speed variations is illustrated in Fig. 21. Wind records taken at the Rutherford and Appleton Laboratories were available and a particular profile was selected to ensure that the wind power did not drop below the minimum value required to overcome the system losses. Fig. 21 shows that while the large system inertia impedes the ability of the system to track the optimum speed, the rms voltage vector magnitude (**V**) is maintained to within 5% during transient conditions without stator resistance compensation. The output frequency is of course a constant set directly by the control structure; an instantaneous frequency of 50Hz is maintained at all times. The steady state optimum operating point tracking is presented in Fig. 22 for several wind velocities up to the rated value. The control described earlier allows tracking of the optimum speed to within an error of 5%. The main source of error is the quantification of mechanical and iron losses in the induction generator and the DC drive that emulates the wind turbine. In the implementation a look-up table of the friction coefficient as a function of the speed is used to increase the accuracy of the tracking, but the iron losses in the machines are not considered.

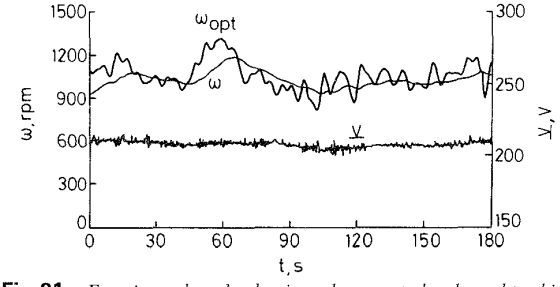

Fig. 21 *Experimental results showing voltage control and speed tracking for operation with a realistic wind profile*

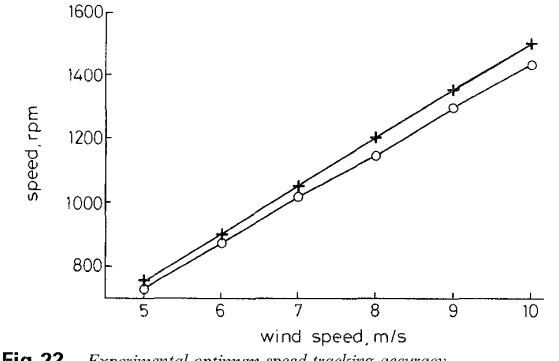

Fig. 22 *Experimental optimum speed tracking accuracy*
+ optimum speed; ∘ generator speed

8 Conclusions

The control of a slip-ring doubly fed induction generator supplying an isolated load at constant voltage and frequency has been presented. The scheme utilises two back-to-back PWM converters in the rotor circuit resulting in low distortion currents, reactive power control and both sub- and super-synchronous operation. A new indirect stator field orientation method has been introduced for the control of the generator. In this method, one of the rotor current components is used to control the machine flux while the other is used to force orientation. The indirect approach ensures that the orientation in both the machine and stator-side converter vector controllers is unaffected by the presence of harmonics on the output voltage. These harmonics are severely exacerbated if the orientation angle is derived from stator voltage measurement. The vector controllers have been validated through the application of both active and reactive load impacts in an experimental rig in which the generator was fed from a speed controlled DC machine. The steady state output voltage regulation is about 3% and increases to 5% during transients typical of real wind profiles. This is obtained without compensation for the resistive voltage drop across the stator.

For variable speed operation from a wind turbine, an auxiliary load is required for power matching. A

scheme for controlling the generator torque via the auxiliary load has been presented in which the generator demand torque is such as to track the optimum shaft speed for maximum energy capture from the wind. These control schemes have also been experimentally implemented and shown to be effective; subject to inertial delay, the system tracks the optimal speed for maximum energy capture while maintaining constant output voltage and output frequency. The investigations have focused upon the control structures necessary to prove the feasibility of a variable speed DFIG feeding an isolated load. Further research will investigate losses, efficiency, optimum reactive power sourcing and the reduction of harmonics via improved PWM schemes and line filtering.

9 References

1 LEONHARD, W.: 'Control of electrical drives' (Springer Verlag, 1985)

2 SMITH, G.A., and NIGIM, K.A.: 'Wind-energy recovery by a static Scherbius induction generator', *IEE Proc. C*, 1981, **128**, (6), pp. 317–324

3 XU, L., and TANG, Y.: 'Stator field oriented control of doubly-excited induction machine in wind power generation system'. 25th Mid West symposium on *Circuit and systems*, Washington, DC, August 1992, pp. 1466–1449

4 XU, L., and CHENG, W.: 'Torque and reactive power control of a doubly fed induction machine by position sensorless scheme', *IEEE Trans. Ind. Applic.*, 1995, **31**, (3)

5 PENA, R., CLARE, J.C., and ASHER, G.M: 'A doubly-fed induction generator using two back-to-back PWM converters and its application to variable speed wind energy system', *IEE Proc. B*, 1996, **143**, (3), pp. 231–241

6 VICATOS, M.S., and TEGOPOULOS : 'Steady state analysis of a doubly-fed induction generator under synchronous operation', *IEEE Trans. Energy Conversion*, 1989, **4**, (3), pp. 495–501

7 BOGALECKA, F.: 'Dynamics of the power control of a double fed induction generator connected to the soft power grid'. ISIE, 1993, Budapest, pp. 509–513

8 TNAMI, S., DIOP, S., and BERTHON, A.: 'Novel control strategy of doubly-fed induction machines', *EPE*, 1995, **1**, pp. 553–558

9 MEBARKY, A., and LIPCZYNSKY, R.T.: 'A novel variable speed constant frequency generation system with voltage regulation', *EPE*, 1995, **2**, pp. 465–471

10 JEONG, S.G., and PARK, M.H.: 'Steady state analysis of a stand alone wound rotor induction generator excited by a PWM inverter'. IEEE IAS Annual Meeting, 1987, Vol. 2, pp. 790–797

11 GOODFELLOW, D., and SMITH, G.A.: 'Control strategy for variable speed wind energy recovery'. Proceedings of 8th British *Wind energy* conference, Cambridge, 1986, pp. 219–228

12 CONNOR, B., and LEITHHEAD, W.E.: 'Investigation of a fundamental trade-off in tracking the $C_{p\ max}$ curve of a variable speed wind turbine'. British *Wind energy* conference, 1993, pp. 313–319

13 CONNOR, B., and LEITHHEAD, W.E.: 'The effect of rotor characteristic on the control of pitch regulated variable speed wind turbines', British *Wind energy* conference, 1994, pp. 67–72

10 Appendix 1: Experimental system ratings

10.1 Wind turbine (emulated by DC machine drive)

Power : 7.5kW

Radius : 3.24m

Rated rotational speed : 296rpm

Rated wind speed : $10\,m\,s^{-1}$

Cut-in speed : $4\,m\,s^{-1}$

Maximum speed : $12\,m\,s^{-1}$

Inertia : $7.5\,kg\,m^2$

Gear box : 5.065

Friction coefficient : $0.06\,Nm\,s\,rad^{-1}$

10.2 Wound rotor induction machine

Power : 7.5kW

Stator Voltage : 415V

Rotor Voltage : 440V

Rated stator current : 19A

Rated rotor current : 11A

R_s : 1.06Ω

R_r : 0.80Ω

L_s : 0.2065H

L_o : 0.0664H (referred to the rotor)

L_r : 0.0810H (referred to the rotor)

L_{ext} : 0.0320H (referred to the rotor)

Pole pairs : 6

Rated speed : 970rpm

Stator-rotor turns ratio n : 1.7

Stator connection : Delta

Rotor connection : Star